ResearchGate

See discussions, stats, and author profiles for this publication at: https://www.researchgate.net/publication/256305137

Self-Assembled Sugar-Substituted Perylene Diimide Nanostructures with Homochirality and High Gas Sensitivity

DATASET *in* ADVANCED FUNCTIONAL MATERIALS · OCTOBER 2012

Impact Factor: 11.81 · DOI: 10.1002/adfm.201200973

CITATIONS
36

READS
65

7 AUTHORS, INCLUDING:

Jianchen hu
National Institute for Materials Science
12 PUBLICATIONS **176** CITATIONS
SEE PROFILE

Charl FJ Faul
University of Bristol
87 PUBLICATIONS **2,078** CITATIONS
SEE PROFILE

Available from: Jianchen hu
Retrieved on: 17 January 2016

Self-Assembled Sugar-Substituted Perylene Diimide Nanostructures with Homochirality and High Gas Sensitivity

Jianchen Hu, Wenfeng Kuang, Ke Deng, Wenjun Zou, Yongwei Huang, Zhixiang Wei,* and Charl F.J. Faul*

A new symmetrical sugar-based perylenediimide derivative PTCDI-BAG is synthesized and its aggregate morphologies and formation mechanisms are studied in detail in the mixed solvent system water/*N*,*N*-dimethylformamide (H_2O/DMF) with changing volume ratios. PTCDI-BAG molecules self-assemble into planar ribbons in 20/80 and 40/60 H_2O/DMF (v/v), but their chiralities are opposite according to recorded circular dichroism (CD) spectra. With a further increase of the water content, only left-handed helical nanowires are obtained in 60/40 and 80/20 H_2O/DMF (v/v) mixtures. By combining density functional theory (DFT) calculations with the experimental investigations, it is proposed that kinetic and thermodynamic factors play key roles in tuning PTCDI-BAG structures and helicity. The formation of the ribbon is thermodynamically controlled in the 20/80 H_2O/DMF system, but kinetically controlled nucleation followed by thermodynamically controlled self-assembly plays the governing roles for the formation of nanoribbons in 40/60 H_2O/DMF. Devices based on single nanoribbons for hydrazine sensing exhibit better performance than nanofiber bundles obtained in this study and achiral nanostructures reported in previous study. This study not only provides an elaborated route to tuning the structures and helicity of PTCDI molecules, but also provides new possibilities for the construction of high-performance nanodevices.

1. Introduction

Control over the self-assembly of elaborately designed organic molecules is a challenging topic for interdisciplinary research in the fields of chemistry, biology, and materials science, as self-assembly provides a spontaneous route towards the generation of well-defined, discrete supramolecular architectures from such molecular components under thermodynamic equilibrium.[1] In particular, there is growing interest in the design of synthetic molecules that are able to self-assemble into compact helical aggregates with specific shape and novel functionalities.[2] However, the process for molecules to self-assemble into helical aggregates, not only in solution but also at surfaces and interfaces, is highly complex. A range of parameters often influences the supramolecular structures of the synthetic molecules, including environmental parameters such as the nature of the solvent, temperature, or any combination of these.[3] Very often, the balance between these parameters is subtle, with seemingly slight changes in experimental conditions leading to drastic changes in the supramolecular structures and helicity. Understanding the kinetic and thermodynamics factors that can control the self-assembly process should therefore lead to pathways for the controlled production of chiral superstructures for high performance devices.[4]

The large number of naturally available chiral molecules provide a rich library of attractive building blocks for use in the design of self-assembling systems.[5] One of the most famous families, after the amino acids, is the sugar-based derivatives in which the sugar entity not only exhibits inherent chiral effects in self-assembly processes, but also supplies hydrogen-bonding interactions for selective solvent interactions.[6] Both of these are driving forces for the formation of the self-assembled helical aggregates. Moreover, helical architectures created from π-systems are of special interest owing to their potential applications as active components in organic electronic devices.[2,7] In particular, various examples of molecules with extended π-conjugated ring systems, such as phthalocyanines,[8]

J. C. Hu, W. K. Kuang, Dr. K. Deng, W. J. Zou, Dr. Y. W. Huang, Prof. Z. X. Wei
National Centre for Nanoscience and Technology
Beijing 100190, China
E-mail: hywei79@126.com; weizx@nanoctr.cn
Dr. Y. W. Huang
Medical College
Henan University
Kaifeng 475004, China
Dr. C. F. J. Faul
School of Chemistry
University of Bristol
BS8 1TS, Bristol, UK
Bristol Centre for Nanoscience and Quantum Information
University of Bristol
Bristol, BS8 1FD, UK

DOI: 10.1002/adfm.201200973

© 2012 WILEY-VCH Verlag GmbH & Co. KGaA, Weinheim

hexabenzocoronenes,[9] and perylene bisimides (PTCDI),[10] have been reported to form π stacks with helical supramolecular structures. We recently showed that asymmetric substitution of a perylene core with a sugar moiety lead to the formation of helical nanowires, where the handedness of the wires depended on the polarity of the solvent from which the wires were prepared.[6e] These proved that such π-conjugated molecules bearing saccharide groups could lead to the development of a robust system for further investigation into the factors governing the formation of helical aggregates.

In the present study, a new symmetrical sugar-based perylene diimide derivative N,N′-bis((4-aminophenyl)-α-D-glucopyranoside)-perylene-3,4:9,10-tetracarboxylbisimide (PTCDI-BAG, **Scheme 1**) was synthesized. Aggregation behavior,

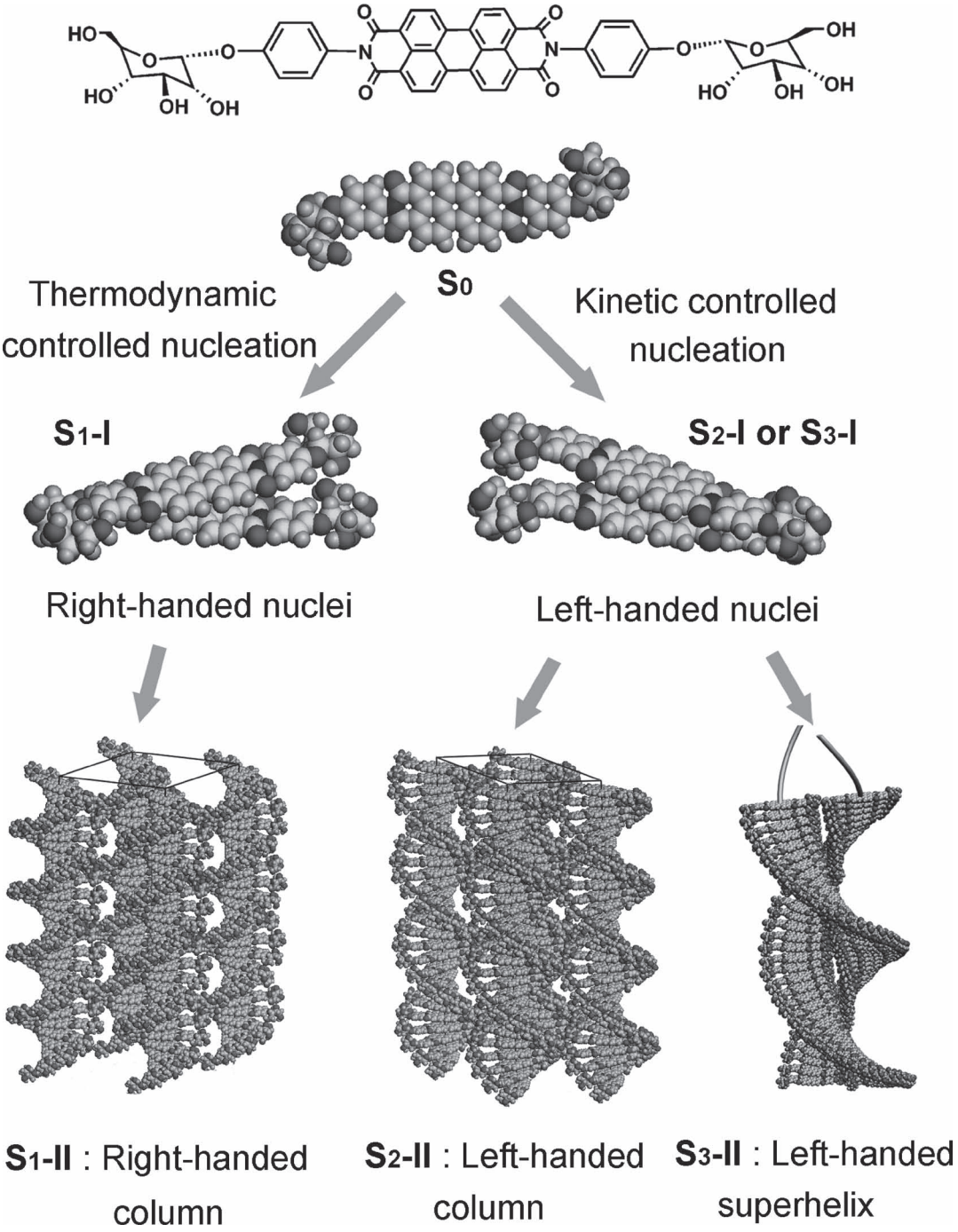

Scheme 1. Molecular structure, kinetic and thermodynamic controlled self-assembly processes of PTCDI-BAG. Right-handed nucleation by thermodynamic controlled process results in right-handed columnar mesophases, while left-handed nucleation by kinetically controlled processes result in left-handed columnar mesophases or left-handed superhelical nanofibers (depending on the ratio of water/DMF).

© 2012 WILEY-VCH Verlag GmbH & Co. KGaA, Weinheim

morphologies and formation mechanism of helical supramolecular aggregates in H2O/DMF mixed solvent systems (with changing volume ratios) were studied in detail. PTCDI was selected as central building block for self-assembly on the basis of geometry (strong, well-studied π–π interactions),[11] and function (optoelectronic properties).[12] The combination here with carbohydrates provide, at the same time, a source of supramolecular chirality for the π-stacking PTCDI molecules. With our results revealing that kinetic and thermodynamic control over the nucleation and self-assembly processes play an important role in tuning the supramolecular structures and their helicity (and thus enabling the formation of well-defined nanoribbons with varying helicity), this study provides a detailed and fundamental understanding of the factors that control the formation of self-assembled nanostructures of chiral-conjugated molecules. Devices based on single nanoribbons for hydrazine sensing exhibited better performance than nanofiber bundles obtained in this study and achiral nanostructures reported in previous study. It is expected that insights gained from this approach will lead to establishing the factors that influence the relationship between nanostructured morphologies and physical properties.

2. Results and Discussion

In order to study the effect and influence of solvents on the kinetic and thermodynamic control of the self-assembly of PTCDI-BAG, a wide range of solvents were investigated. The result revealed that the complex has high solubility only in DMF, and is practically insoluble in water, ethanol, methanol, chloroform, and dichloromethane. Herein, we therefore selected water and DMF to form H_2O/DMF mixed solvent systems (with varying volume ratio) to further study solvent impact on the structures and helicity of PTCDI-BAG aggregates.

The morphologies of PTCDI-BAG in H_2O/DMF mixed solvents (with different volume ratios at a concentration of 0.06 mg·mL^{-1}) were examined by transmission electron microscopy (TEM). As shown in **Figure 1**a, planar ribbons with an

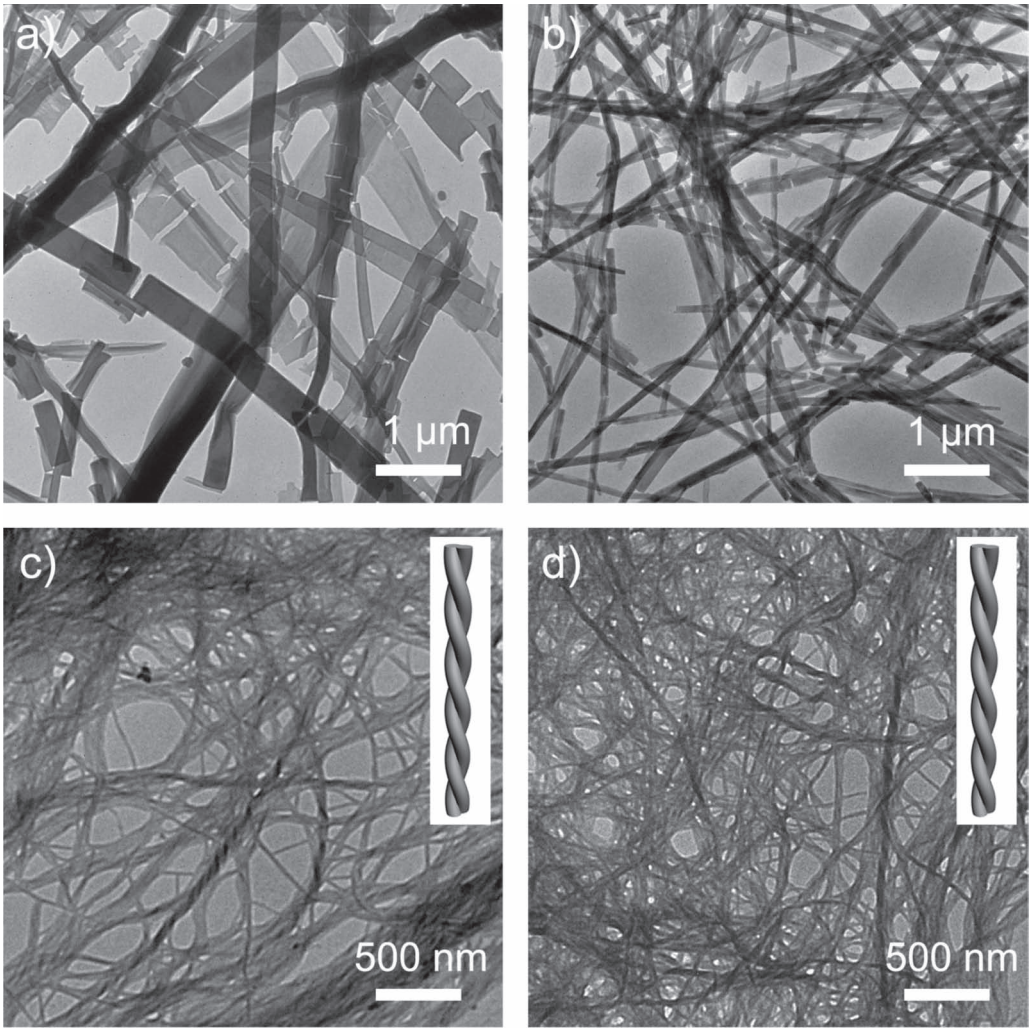

Figure 1. TEM images of PTCDI-BAG nanostructures obtained from H_2O/DMF mixed solvents (0.06 mg·mL^{-1}) with different volume ratios of (a) 20/80; (b); 40/60 (c) 60/40 and (d) 80/20. The inserts in c and d indicate the left-handed helical sense of the nanofibers. The samples were prepared after an equilibration period of 48 h at room temperature.

© 2012 WILEY-VCH Verlag GmbH & Co. KGaA, Weinheim

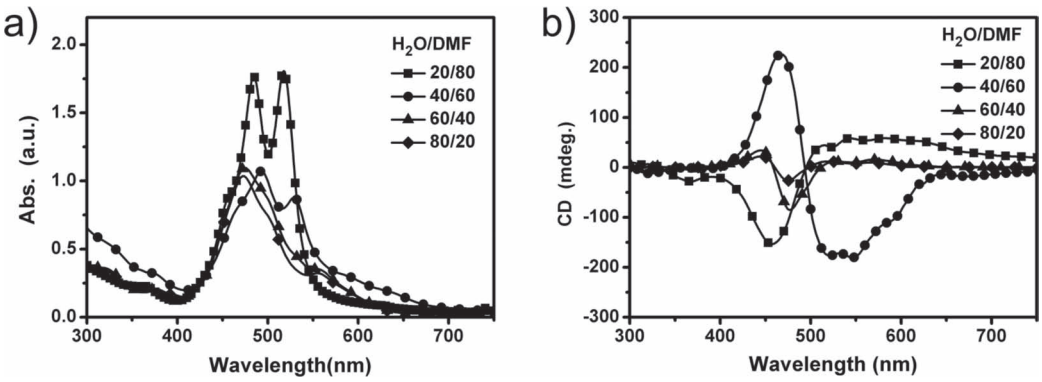

Figure 2. (a) UV-Vis and (b) CD spectra of the PTCDI-BAG molecules in different volume ratios of H_2O/DMF mixed solvents. The samples were characterized after an equilibration period of 48 h at room temperature.

average diameter of ca. 500 nm were generated in 20/80 H_2O/DMF (v/v). With increasing content of water up to 40 vol% planar ribbons were still obtained, but the diameters of ribbons progressively decreased to 100–300 nm (Figure 1b). When the water content exceeded 40 vol%, nanofibers with diameters smaller than 50 nm were obtained (i.e., in the 60/40 and 80/20 H_2O/DMF systems, Figure 1c and d).

Interestingly, left-handed helical structures were clearly observed in Figure 1c and d, indicating that the chiral groups played an important role in the formation of nanostructures. These results suggest that the content of water in the combined solvent system has a great impact on the variation in the aggregated morphologies of PTCDI-BAG. The morphologies observed by TEM were further confirmed by scanning electron microscope (SEM) investigation, proving that the morphologies were uniform in all the samples (see Figure S1 in Supporting Information).

To understand the aggregation of PTCDI-BAG in H_2O/DMF mixtures, UV-Vis absorption and CD spectra were recorded for various H_2O/DMF volume ratios (**Figure 2**). When 20 vol% H_2O was gradually added to the DMF solution, the absorption peak at 490 nm, compared to that at 518 nm, was dramatically enhanced, indicating the onset of aggregation.[13] With further H_2O addition (reaching 40 vol%), the intensity ratio continued to increase (Figure 2a). When the content of water exceeded 40 vol%, a new shoulder peak was observed at approximately 550 nm. This pronounced absorption band at longer wavelengths is typically a sign of effective π–π interactions in a co-facial configuration of molecular stacking, which was further supported by fluorescence spectra as shown in Figure S2.[14]

Accordingly, intense Cotton effects were observed for PTCDI-BAG molecules in H_2O/DMF mixtures. As shown in Figure 2b, the CD spectrum of PTCDI-BAG in 20/80 H_2O/DMF(v/v) showed a bisignate CD signal with a negative CD signal at 450 nm and a positive CD signal at ca. 525 nm (crossover at 490 nm). A bisignate CD signal is indicative of chiral excitonic coupling that arises when chromophores are aggregated with their transition dipoles oriented in a helical fashion.[14] The bisignate negative/positive signal with increasing wavelength indicates that the PTCDI-BAG molecules adopted a right-handed helical arrangement.[15]

With an increase in H_2O content to 40%, PTCDI-BAG aggregation exhibited the opposite behavior in terms of chirality, and produced mirror image Cotton effects. A positive CD peak at 450 nm and a negative CD peak at ca. 525 nm were found in the CD spectrum of PTCDI-BAG in 40/60 H_2O/DMF (v/v) (Figure 2b). The position of the CD bands changed and was less intense with further increases of the H_2O content to 60 and 80 vol%. The bisignate signal, characterized by a change from positive to negative with increasing wavelength, indicates a left-handed or counter-clockwise helical arrangement of the transition dipoles,[16] which was consistent with the TEM and SEM observations (Figure 1c and 1d) as discussed above.

To further trace the effect of the solvents on the aggregation behavior and elucidate the self-assembly mechanism of the planar ribbons, time-dependent UV-Vis and CD spectra of PTCDI-BAG molecules in different H_2O/DMF (v/v) ratios were recorded to monitor the self-assembly process. As shown in **Figure 3**a, the intensity ratio of the absorption peaks at 490 nm and 518 nm was gradually enhanced with the extension of time from 0 to 48 h, which indicated that increased π-π stacking occurred between PTCDI-BAG molecules in 20/80 H_2O/DMF water (v/v).[6e,15]

Accordingly, there was almost no CD signal at the initial state, and a weak bisignate CD signal with a negative CD peak at 450 nm and a positive peak at 525 nm that developed in the CD spectrum after 2 h. The intensity was dramatically enhanced with the extension of time to 48 h (Figure 3b). The CD spectra clearly showed that PTCDI-BAG molecules adopted a right-handed helical arrangement in the nucleation stage of the assembly process. The nuclei further aggregated into high-level aggregates by this preferred right-handed way, accompanied by an enhancement in CD signal until supramolecular structures, namely planar nanoribbons, were formed. This progression and consolidation of the initial nucleation step into the same right-handed self-assembled ribbons in 20/80 H_2O/DMF provided clear evidence of a thermodynamically controlled assembly process.[17]

However, some significant changes were observed in the UV-Vis and CD spectra of PTCDI-BAG molecules with an increase in water content to 40% in DMF. As shown in the UV/Vis data (Figure 3c), the intensity ratio of the absorption peak at 490 nm to that at 518 nm was further increased compared to that in 20/80 H_2O/DMF. Moreover, a shoulder peak at ca. 600 nm was dramatically enhanced, which indicates a much higher degree of π–π stacking between PTCDI-BAG molecules

© 2012 WILEY-VCH Verlag GmbH & Co. KGaA, Weinheim

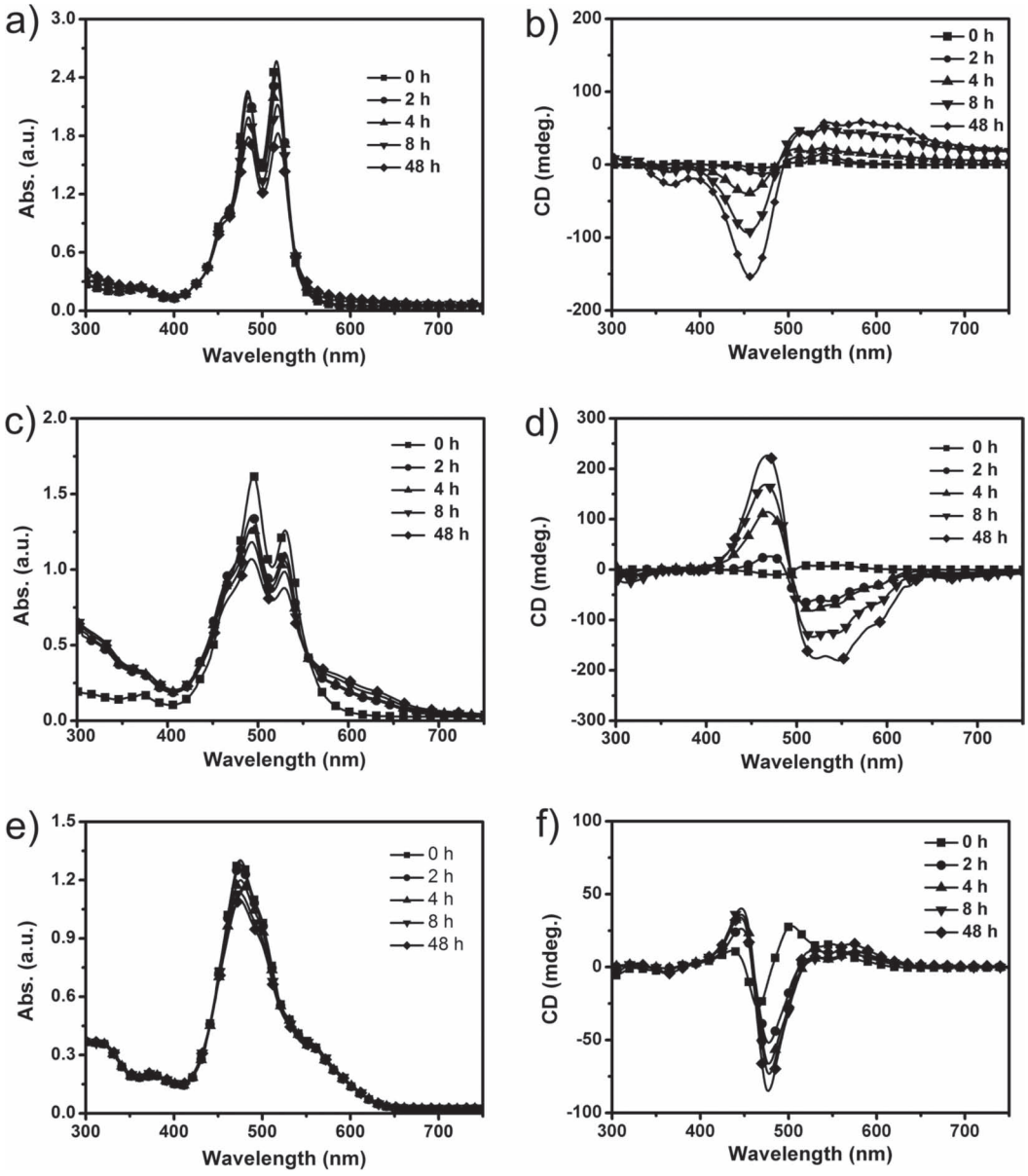

Figure 3. Time-dependent (a, c, e) UV-Vis and (b, d, f) CD spectra of PTCDI-BAG molecules in 20/80, 40/60, 60/40 H_2O/DMF (v/v) mixed solvents, respectively.

in the 40/60 H_2O/DMF system. Recording the CD spectrum in 40/60 H_2O/DMF solution showed weak CD signals in the initial stage of the aggregation process (Figure 3d). By these weak CD signals it was difficult to determine the handness, but TEM image clearly showed left-handed nuclei at the initial stage (See later in **Figure 4**a). With the extension of time to more than 2 h, the CD signals were red shifted significantly to 450 nm and 525 nm, and a clear left-handed helix could be determined by CD signals. This result indicated the nuclei formed in the 40/60 H_2O/DMF system were metastable, and that this state was most probably kinetically controlled. The metastable nuclei evolved into a stable supramolecular state of left-handed ribbons, which was achieved via a thermodynamically controlled process.[3e] The CD results obtained here are similar to that in 60/40 H_2O/DMF (Figure 3f), also indicating a left-handed helical arrangement of the aggregated assemblies.

In the 60/40 H_2O/DMF system, although the development of the CD spectra are initially similar to that of the 40/60 H_2O/DMF system, it was not possible to reach a thermodynamically stable state due to strong aggregation at the initial stage of the assembly process (as indicated by its UV spectrum, Figure 3e). The spectra at 80/20 H_2O/DMF were similar to that of 60/40 (Figure S3 in Supporting Information).

To further elucidate the formation mechanism of the planar ribbons, time-dependent evolution of PTCDI-BAG aggregation in 40/60 H_2O/DMF was characterized in detail by TEM. As shown in Figure 4a, when 40 vol% water was added into the DMF solution, PTCDI-BAG molecules rapidly aggregated

© 2012 WILEY-VCH Verlag GmbH & Co. KGaA, Weinheim

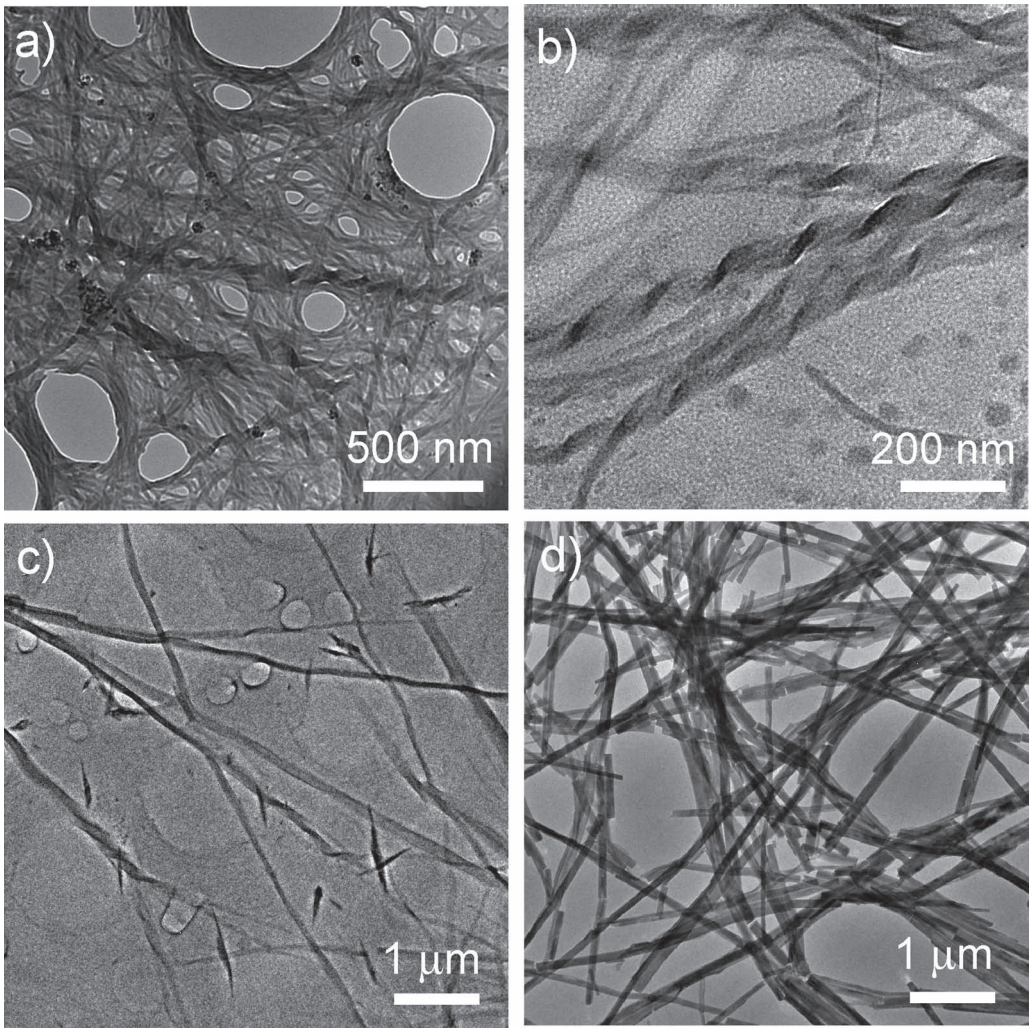

Figure 4. Time-dependent evolution of PTCDI-BAG nanostructures in H_2O/DMF binary solutions (40/60, v/v) at concentration of 0.06 mg·mL^{-1} with different time intervals of (a) 0 h; (b) 1 h; (c) 4 h; (d) 48 h.

and further self-assembled into left-handed nanowires by virtue of the π–π stacking between the perylene groups. The elementary wires then tightly packed together, driven by the hydrogen bonding between the sugar moieties, to form bundles as recorded in Figure 4b and 4c. These bundles align and pack side-by-side, thereby forming planar ribbons (Figure 4d). Although individual wires are curved and seemingly flexible, the ribbons composed of the wires are hard and brittle. A similar observation was also reported for the glycouril-based gelating system by Menger et al.[16] and aryl–glycolipids system by Shimizu et al.[17] It should be noted that although the ribbons formed in 40/60 H_2O/DMF did not show any chiral morphology, obvious Cotton effects were observed, suggesting ribbon-like structures were formed by organized helical stacking of PTCDI molecules. The results from 20/80 H_2O/DMF are illustrated in Figure S4 in Supporting Information. The nanoribbons at 20/80 H_2O/DMF were formed by a very similar process, but their preliminary nanowires are right-handed, which is consistent with the results of CD spectra (Figure 3b).

The crystalline structure of the nanoribbons was further investigated by high resolution transmission electron microscopy (HRTEM), selected-area electron diffraction (SAED) and X-ray diffraction (XRD). HRTEM showed highly ordered structures with an inter-columnar distance of *ca.* 3.0 nm (**Figure 5**a). The XRD patterns (Figure 5c) displayed a series of sharp diffraction lines, implying the formation of a crystalline structure. Detailed analysis showed that the crystalline phase of these nanoribbons were orthorhombic, with cell parameters of a = 23.84 Å, b = 6.78 Å, c = 30.06 Å, and γ = 129.2°. This result was further supported by SAED (Figure 5b). Electron diffraction results showed a *d*-spacing of 3.6 Å in the longitudinal nanoribbon direction, which suggests that the molecules are oriented with their long axis perpendicular to the ribbon and the π-π stacking direction parallel to the ribbon. The 3.6 Å π–π stacking distance between two adjacent molecular planes is consistent with that of other PTCDI molecules.[18] Combining this information with the helical twist of PTCDI-BAG molecules, a molecular stacking model in nanoribbons were

© 2012 WILEY-VCH Verlag GmbH & Co. KGaA, Weinheim

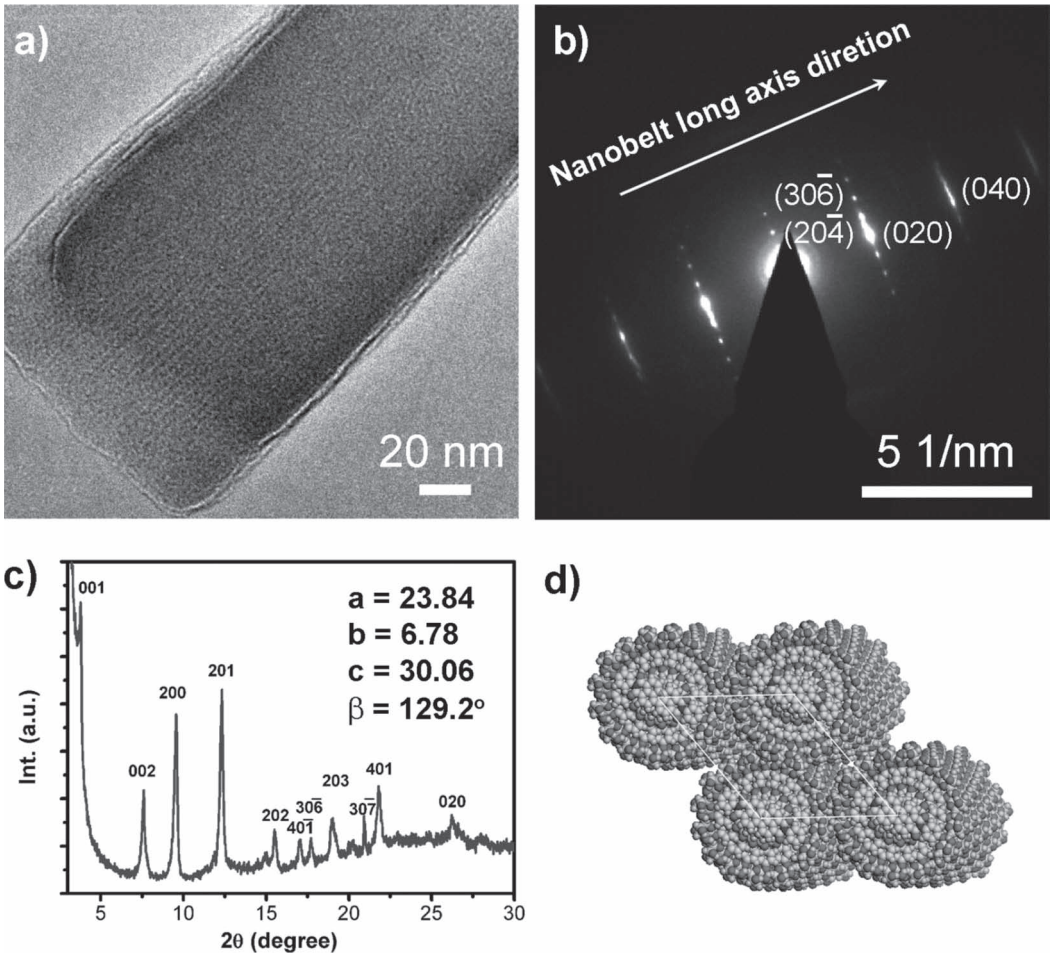

Figure 5. (a) HRTEM image with the π-stacking distance indicated, (b) SEAD pattern of a single nanoribbon in H_2O/DMF (40/60, v/v) binary solutions, (c) XRD pattern, and (d) mesophase model of the nanoribbon. The sample was obtained at a concentration of 0.06 mg·mL^{-1} with time intervals of 48 h.

proposed, as shown in Figure 1 and Figure 5d. A very similar crystalline structures was obtained from the SAED of nanoribbon obtained for 20/80 H_2O/DMF system (see Figure S5 in Supporting Information). Since crystal structure analysis is crucial to understanding microstructure-function relationships, based on the presented data, high charge carrier transport is highly likely for PTCDI-BAG nanoribbons (see later).[19]

Keeping the presented data in mind, we can now proceed to detailed analyses of the assembly processes involved. The PTCDI-BAG molecule in our study is unique in that its structure consists of a hydrophobic perylene scaffold with hydrophilic galactosyl residues on either side. When dissolved in DMF, both the perylene scaffold and galactosyl residues exhibit good solubility (Scheme 1, S_0 state). Upon adding a small amount of water (20 vol%) into PTCDI-BAG DMF solution, the perylene diimide scaffold that has low solubility in water will aggregate into nuclei (Scheme 1, S_1-I state) with right-handed helical arrangement at first under thermodynamic control. The formed nuclei then self-assemble into nanoribbons with a right-handed helical architecture (Scheme 1, S_1-II state) by π–π stacking of the perylene scaffold via a thermodynamically controlled process.

However, when a relative large amount of water (40 vol%) is added into the DMF solution, PTCDI-BAG molecules aggregate rapidly into nuclei with a left-handed helical arrangement (Scheme 1, S_2-I state) via a kinetically controlled process due to the dramatic decrease in solubility. The nuclei then evolve into stable nanoribbons by a slow self-assembly process. Owing to the sergeant and soldiers rule,[1b] the helicity of nanoribbons (ascertained by CD investigations) was left-handed, following the helicity of kinetically controlled nucleation process. This deduction was further confirmed by increasing the water ratios to 60% and 80%, and in both cases left-handed helical stacking (Scheme 1, S_3-I state) and left-handed helical nanofibers were obtained (Scheme 1, S_3-II state).

DFT calculations were performed to investigate the thermodynamic process to form such chiral architectures. Exploring different orientations of the end galactosyl groups, there are three possible geometric configurations available for PTCDI-BAG (Figure S6 in Supporting Information). DFT optimizations show that the most energetically preferable geometry is the one in which both the end galactosyl groups exhibit a preferred anti-clockwise orientation relative to the center of

© 2012 WILEY-VCH Verlag GmbH & Co. KGaA, Weinheim

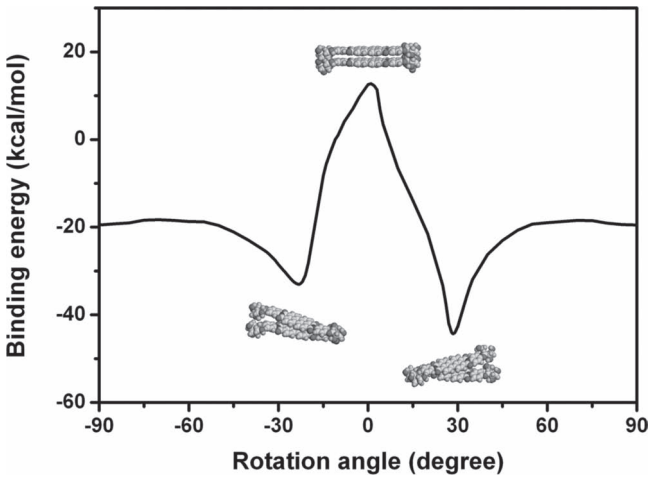

Figure 6. Simulations to investigate the energy dependence on rotation of the PTCDI-BAG upper molecules in a stacked dimer. The upper molecule rotates gradually with the rotation angle changing from 0° to 90° (right-handed)/from 0° to –90° (left-handed). The binding energy equals the total energy of the dimer minus the energy of the two separate molecules. The positive binding energy means the system is unstable, whereas the negative binding energy means the system is stable.

the molecule. Thus, it is reasonable to consider such a geometry as the preferred and stable building block in the chiral architecture.

Using the optimized structures, stable structures of a molecular dimer were then investigated. The molecules preferred to stack with a vertical distance of 3.5 Å, which is obtained from the experimental XRD and SEAD data. It also suggests that the π–π interaction plays an essential role in the formation of the nucleation. The galactosyl groups, however, should affect the chirality of the helix. Due to the steric hindrance of the galactosyl groups, the adjacent molecules should rotate a certain angle to reach the conformation with the minimal system energy. With the molecules coaxially arranged, the energy dependence on rotation angle was calculated and is presented in **Figure 6**.

It shows that, at first, where the two molecules are stacked in a totally eclipsed fashion and the rotation angle = 0°, the binding energy of the system is positive, which means the system is unstable. During the subsequent rotation process, the upper molecule rotates gradually with the rotation angle changing from 0° to 90° (right-handed) and from 0° to –90°(left-handed), and the binding energy of the system changes from positive to negative; that is, the system becomes more stable compared to the starting structure. In Scheme 1, the structure with the right-handed rotation angle 28.5° has the lowest binding energy, indicating that such a structure is the most stable. This agrees very well with our experimental observation of right-handed chirality of the nuclei.

It is interesting to note that at a rotation angle = –23.3° (left-handed), the system has a less stable local minimum. This result suggests that although it is not the most thermodynamically preferred state, it still can occur kinetically, thus providing theoretical support for our experimental observation of the left-handed nuclei at higher water content. As nucleation processes normally need to overcome a free energy barrier,[20] we suggest kinetic factors determined the formation of left-handed nuclei by overcoming smaller free energy barriers than that of right-handed nuclei. When the water content is higher than 40%, fast aggregation of PTCDI-BAG molecules helped the formation and trapping of the left-handed helical stacking at the initial stages.

As organic semiconductor materials, homochiral π-conjugated molecules have exhibited increased charge-carrier mobilities as a result of the higher molecular order imparted by the helical stacking arrangement.[10a,21] Therefore, the change in conductivity of a single nanoribbon formed at 40/60 H_2O/DMF and nanowire bundles formed at 60/40 H_2O/DMF was recorded in hydrazine vapor using a two-probe method (**Figure 7**).

The devices were prepared with architectures as in Figure 7a and b, according to the method by Hu et al.[22] As shown in Figure 7c and d, compared to the conductivity in vacuum, an approximately 4-orders-of-magnitude decrease in resistance is observed for the nanoribbon upon exposure to hydrazine vapor (10 ppm). However, only a 2–3 order-of-magnitude decrease was obtained for nanofiber bundles. Moreover, compared to achiral nanostructures, chiral nanoribbons in this study exhibited one order increase in their sensitivity.[23] The results indicate that the high crystallinity and single-handed chirality of nanoribbon is helpful to increase their properties for gas sensing because of better organization of PTCDI-BAG molecules.

3. Conclusions

A new sugar-based perylenediimide derivative PTCDI-BAG was synthesized and its aggregate morphologies and formation mechanism in H_2O/DMF solvent mixtures with changing volume ratios were studied in detail. The results indicated PTCDI-BAG molecules self-assembled into planar ribbons in 20/80 and 40/60 H_2O/DMF (v/v), while left-handed helical nanowires were obtained in 60/40 and 80/20 H_2O/DMF (v/v). Detailed investigation into the self-assembly mechanism revealed that the formation of the ribbons was thermodynamically controlled in 20/80 H_2O/DMF, but a kinetically controlled nucleation and then thermodynamically controlled self-assembly process was responsible for the formation of nanoribbons in 40/60 H_2O/DMF (and higher H_2O ratios). These kinetic and thermodynamic factors determined the observed opposite helical stacking in the two different nanoribbons, which was furthermore supported by DFT calculations. Demonstration devices for hydrazine sensing based on single nanoribbons exhibited better performance than nanofiber bundle devices. This study not only provides an elaborated pathway to tuning the structures and helicity of PTCDI molecules, but also provides the possibility to construct high-performance nanodevice utilizing easily accessible control mechanisms.

© 2012 WILEY-VCH Verlag GmbH & Co. KGaA, Weinheim

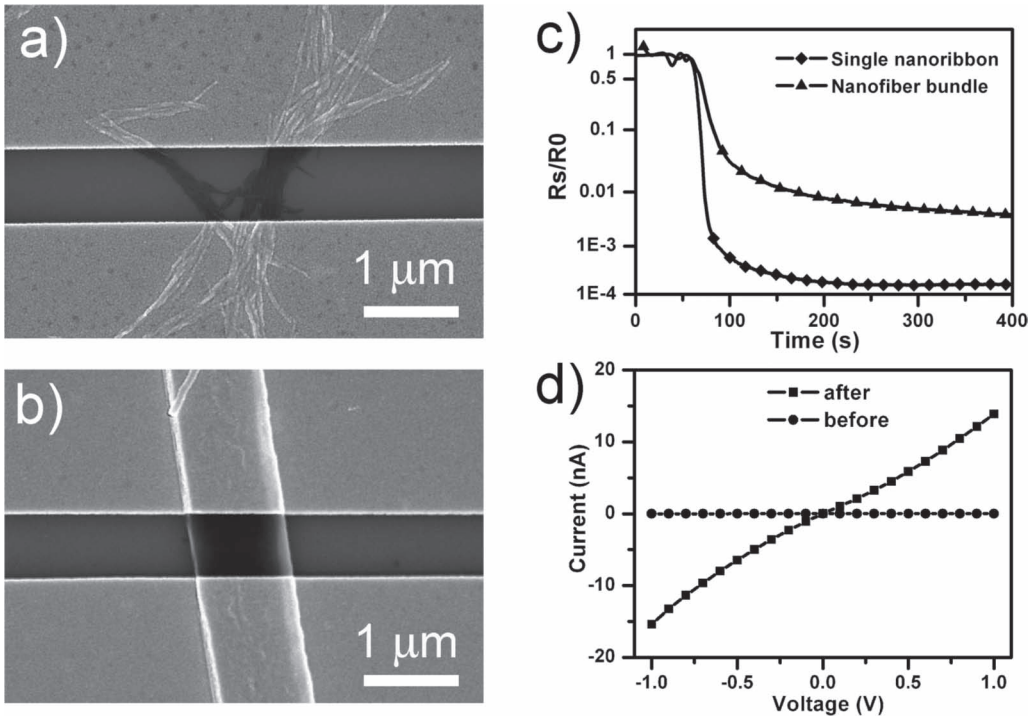

Figure 7. Sensing properties of helical nanofibers and nanoribbons in response to exposure to hydrazine. a) and b) SEM images of the device. based on nanofiber bundles and a single nanoribbon, respectively; c) sensing properties of a) and b) after the injection of hydrazine; d) I-V curves of nanoribbon before and after the injection of hydrazine. Nanofibers and nanoribbons were obtained from H_2O/DMF ratios of 60/40 and 40/60, respectively.

4. Experimental Section

Preparation of PTCDI-BAG Nanostructures: The synthesis and characterization are provided in the Supplementary Information. To obtain the supramolecular structures, PTCDI-BAG (2 mg, 2.23×10^{-3} mmol) was firstly dissolved in 2 mL DMF to obtain a stock solution at a concentration of 1 mg·mL^{-1}, and was then diluted to the required concentration. Water was then injected into DMF solutions of PTCDI-BAG with H_2O/DMF volume ratios of 20/80, 40/60, 60/40, and 80/20 respectively, with the final PTCDI-BAG concentrations were kept as a constant of 0.06 mg·mL^{-1}. After vigorous stirring for 10 minutes, the samples were kept stationary to self-assemble for different time intervals at room temperature.

Methods: ^{1}H NMR was acquired using a Bruker 400 MHz NMR spectrometer. Solid-state ^{13}C NMR was acquired using a Bruker AVANCE III 400 MHz NMR spectrometer. Circular dichroism (CD) measurements were conducted on a JASCOJ-810 spectrometer at room temperature. UV-Vis adsorption spectra were recorded on Perkin-Elmer Lamda 950 UV-Vis spectroscopy. Fluorescence spectra were recorded by using a Perkin-Elmer LS 55 luminescence spectrometer. X-ray diffraction measurements were carried out on a Japan Rigaku D/max-2500 rotation anode X-ray diffractometer equipped with graphite monochromatized Cu Kα radiation (λ = 1.5406 Å). The samples for X-ray diffraction measurement were prepared on glass cover slips by drop casting, followed by drying at room temperature. TEM measurement was acquired using a TECHNAI G2 20 S-TWIN transmission electron microscopy (200 KV). Samples were prepared by dropping a sample (1 μL) on carbon-film-covered 200 mesh grids, followed by drying in air.

Supporting Information

Supporting Information is available from the Wiley Online Library or from the author.

Acknowledgements

J.C.H. and W.F.K. contributed equally to this work. The authors gratefully acknowledge the National Natural Science Foundation of China (Nos: 91027031, 20933008), the Ministry of Science and Technology of China (Nos: 2009CB930400, 2012CB933001, 2010DFB63530) and Chinese Academy of Sciences (CAS) for financial support. C.F.J.F. thanks the Royal Society and CAS for generous support through an International Joint Project (travel and cooperation with China).

Received: April 5, 2012
Published online: June 14, 2012

[1] a) J. M. Lehn, *Proc. Natl. Acad. Sci. USA* **2002**, *99*, 4763–4768; b) F. J. M. Hoeben, P. L. Jonkheijm, E. W. Meijer, A. P. H. J. Schenning, *Chem. Rev.* **2005**, *105*, 1491–1546; c) J. H. Ryu, L. Tang, E. Lee, H. J. Kim, M. Lee, *Chem. Eur. J.* **2008**, *14*, 871–881; d) A. Lohr, T. Gress, M. Deppisch, M. Knoll, F. Würthner, *Synthesis*, **2007**, *19*, 3037–3082.

[2] a) K. Maeda, E. Yashima, *Top. Curr. Chem.* **2006**, *265*, 47–88; b) C. L. Lee, C. Grenier, E. W. Meijer, A. P. H. J. Schenning, *Chem. Soc. Rev.* **2009**, *38*, 671–683; c) M. Yang, N. A. Kotov, *J. Mater. Chem.* **2011**, *21*, 6775–6792; d) V. Percec, M. Peterca, T. Tadjiev, X. B. Zeng, G. Ungar, P. Leowanawat, E. Aqad, M. R. Imam, B. M. Rosen, U. Akbey, R. Graf, S. Sekharan, D. Sebastiani, H. W. Spiess, P. A. Heiney, S. D. Hudson, *J. Am. Chem. Soc.* **2011**, *133*, 12197–12219.

[3] a) H. Nakashima, M. Fujiki, J. R. Koe, M. Motonaga, *J. Am. Chem. Soc.* **2001**, *123*, 1963–1969; b) A. Brizard, C. Aimé, T. Labrot, I. Huc, D. Berthier, F. Artzner, B. Desbat, R. Oda, *J. Am. Chem. Soc.* **2007**, *129*, 3754–3762; c) R. S. Johnson, T. Yamazaki, A. Kovalenko,

© 2012 WILEY-VCH Verlag GmbH & Co. KGaA, Weinheim

H. Fenniri, *J. Am. Chem. Soc.* **2007**, *129*, 5735–5743; d) J.-H. Ryu, L. Tang, E. Lee, H.-J. Kim, M. Lee, *Chem. Eur. J.* **2008**, *14*, 871–881; e) J. Cui, A. Liu, Y. Guan, J. Zhang, Z. Shen, X. Wan, *Langmuir*, **2010**, *26*, 3615–3622.

[4] a) A. Lohr, M. Lysetska, F. Würthner, *Angew. Chem. Int. Ed.* **2005**, *44*, 5071–5074; b) P. A. Korevaar, S. J. George, A. J. Markvoort, M. M. J. Smulders, P. A. J. Hilbers, A. P. H. J. Schenning, T. F. A. Greef, E. W. Meijer, *Nature*, **2012**, *481*, 492–496.

[5] a) J. D. Hartgerink, E. Beniash, S. I. Stupp, *Proc. Natl. Acad. Sci. USA* **2002**, *99*, 5133–5138; b) T. Muraoka, H. Cui, S. I. Stupp, *J. Am. Chem. Soc.* **2008**, *130*, 2946–2947; c) L. Hsu, G. L. Cvetanovich, S. I. Stupp, *J. Am. Chem. Soc.* **2008**, *130*, 3892–3899; d) O. S. Lee, S. I. Stupp, G. Schatz, *J. Am. Chem. Soc.* **2011**, *133*, 3677–3683.

[6] a) S. Tamaru, M. Nakamura, M. Takeuchi, S. Shinkai, *Org. Lett.* **2001**, *3*, 3631–3634; b) T. Shimizu, M. Masuda, H. Minamikawa, *Chem. Rev.* **2005**, *105*, 1401–1443; c) T. F. Lin, R. M. Ho, C. H. Sung, C. S. Hsu, *Chem. Mater.* **2008**, *20*, 1404–1409; d) J. Zheng, W. Qiao, X. Wan, J. P. Gao, Z. Y. Wang, *Chem. Mater.* **2008**, *20*, 6163–6168; e) Y. Huang, J. Hu, W. Kuang, Z. Wei, C. F. J. Faul, *Chem. Commun.* **2011**, *47*, 5554–5556; f) K.-R. Wang, H.-W. An, L. Wu, J.-C. Zhang, X.-L. Li, *Chem. Commun.* **2012**, *48*, 5644–5646.

[7] a) D. B. Amabilino, J. Veciana, *Top. Curr. Chem.* **2006**, *265*, 253–302; b) H. Maeda, Y. Ito, Y. Haketa, N. Eifuku, E. Lee, M. Lee, T. Hashishin, K. Kaneko, *Chem. Eur. J.* **2009**, *15*, 3706–3719.

[8] a) H. Engelkamp, S. Middlebeek, R. J. M. Nolte, *Science* **1999**, *284*, 785–788; b) W. Li, T. Aida, *Chem. Rev.* **2009**, *109*, 6047–6076.

[9] a) J. Wu, M. D. Watson, L. Zhang, Z. Wang, K. Müllen, *J. Am. Chem. Soc.* **2004**, *126*, 177–186; b) T. Yamamoto, T. Fukushima, A. Kosaka, W. Jin, Y. Yamamoto, N. Ishii, T. Aida, *Angew. Chem. Int. Ed.* **2008**, *47*, 1672–1675.

[10] a) V. Dehm, Z. Chen, U. Baumeister, P. Prins, L. D. A. Siebbeles, F. Würthner, *Org. Lett.* **2007**, *9*, 1085–1088; b) Y. Huang, Y. Yan, B. M. Smarsly, Z. Wei, C. F. J. Faul, *J. Mater. Chem.* **2009**, *19*, 2356–2362; c) D. Franke, M. Vos, M. Antonietti, N. A. J. M. Sommerdijk, C. F. J. Faul, *Chem. Mater.* **2006**, *18*, 1839–1847; d) A. P. H. J. Schenning, J. V. Herrikhuyzen, P. Jonkheijm, Z. Chen, F. Würthner, E. W. Meijer, *J. Am. Chem. Soc.* **2002**, *124*, 10252–10253; e) P. Jonkheijm, N. Stutzmamn, Z. Chen, D. M. De L. Leeuw, E. W. Meijer, A. P. H. J. Schenning, F. Würthner, *J. Am. Chem. Soc.* **2006**, *128*, 9535–9540.

[11] a) L. Zang, Y. Che, J. S. Moore, *Acc. Chem. Res.* **2008**, *41*, 1596–1608; b) Y. Liu, K. R. Wang, D. S. Guo, B. P. Jiang, *Adv. Funct. Mater.* **2009**, *19*, 2230–2235; c) Y. Che, X. Yang, G. Liu, C. Yu, H. Ji, J. Zuo, J. Zhao, L. Zang, *J. Am. Chem. Soc.* **2010**, *132*, 5743–5750; d) M. Huang, U. Schilde, M. Kumke, M. Antonietti, H. Colfen, *J. Am. Chem. Soc.* **2010**, *132*, 3700–3707; e) F. Würthner, *Chem. Commun.* **2004**, 1564–1579.

[12] a) W. Wang, A. D. Shaller, A. D. Q. Li, *J. Am. Chem. Soc.* **2008**, *130*, 8271–8279; b) R. Schmidt, J. H. Oh, Y. S. Sun, M. Deppisch, A. M. Krause, K. Radacki, H. Braunschweig, M. Könemann, P. Erk, Z. Bao, F. Würthner, *J. Am. Chem. Soc.* **2009**, *131*, 6215–6228; c) M. L. Tang, J. H. Oh, A. D. Reichardt, Z. Bao, *J. Am. Chem. Soc.* **2009**, *131*, 3733–3740; d) M. C. R. Delgado, E. G. Kim, D. A. da S. Filho, J. L. Bredas, *J. Am. Chem. Soc.* **2010**, *132*, 3375–3387; e) A. S. Molinari, H. Alves, Z. Chen, A. Facchetti, A. F. Morpurgo, *J. Am. Chem. Soc.* **2009**, *131*, 2462–2463.

[13] W. Wang, W. Wan, H. H. Zhou, S. Q. Niu, A. D. Q. Li, *J. Am. Chem. Soc.* **2003**, *125*, 5248–5249.

[14] F. Würthner, C. Thalacker, S. Diele, C. Tschierske, *Chem. Eur. J.* **2001**, *7*, 2245–2253.

[15] F. Würthner, Z. Chen, F. J. M. Hoeben, P. Osswald, C. C. You, P. Jonkheijm, J. V. Herrikhuyzen, A. P. H. J. Schenning, P. P. A. M. van derSchoot, E. W. Meijer, E. H. A. Beckers, S. C. J. Meskers, R. A. J. Janssen, *J. Am. Chem. Soc.*, **2004**, *126*, 10611–10618.

[16] a) M. Kolbel, F. M. Menger, *Chem. Commun.* **2001**, 275–276; b) M. Kolbel, F.M. Menger, *Adv. Mater.* **2001**, *13*, 1115–1119.

[17] G. John, J. H. Jung, M. Masuda, T. Shimizu, *Langmuir* **2004**, *20*, 2060–2065.

[18] H. F. Ji, R. Majithia, X. Yang, X. Xu, K. More, *J. Am. Chem. Soc.* **2008**, *130*, 10056–10057.

[19] a) Q. Bao, B. M. Goh, B. Yan, T. Yu, Z. Shen, K. P. Loh, *Adv. Mater.* **2010**, *22*, 3661–3666; b) Y. Huang, L. Fu, W. Zou, F. Zhang, Z. Wei, *J. Phys. Chem. C* **2011**, *115*, 10399–10404; c) Y. Huang, R. Yuan, S. Zhou, *J. Mater. Chem.* **2012**, *22*, 883–888; d) Y. Huang, L. Fu, W. Zou, F. Zhang, *New J. Chem.* **2012**, *36*, 1080–1084.

[20] A. R. Fersht, *Curr. Opin. Struct. Biol.* **1997**, *7*, 3–9.

[21] X. L. Feng, V. Marcon, W. Pisula, M. R. Hansen, J. Kirkpatrick, F. Grozema, D. Andrienko, K. Kremer, K. Müllen, *Nat. Mater.* **2009**, *8*, 421–426.

[22] L. Jiang, J. Gao, E. Wang, H. Li, Z. Wang, W. P. Hu, *Adv. Mater.* **2008**, *20*, 2735–2740.

[23] Y. Huang, B. Quan, Z. Wei, G. Liu, L. Sun, *J. Phys. Chem. C.* **2009**, *113*, 3929–3933.

© 2012 WILEY-VCH Verlag GmbH & Co. KGaA, Weinheim